ACS OMEGA

http://pubs.acs.org/journal/acsodf

Article

Low-Cost Silicon Phthalocyanine as a Non-Fullerene Acceptor for Flexible Large Area Organic Photovoltaics

Chithiravel Sundaresan, Mário C. Vebber, Jaclyn L. Brusso, Ye Tao, Salima Alem,* and Benoît H. Lessard*

Cite This: *ACS Omega* 2023, 8, 1588−1596

Read Online

ACCESS | Metrics & More | Article Recommendations | Supporting Information

ABSTRACT: We demonstrate large-area (1 cm^2) organic photovoltaic (OPVs) devices based on bis(tri-n-butylsilyl oxide) silicon phthalocyanine $(3BS)_2$-SiPc as a non-fullerene acceptor (NFA) with low synthetic complexity paired with poly(3-hexylthiophene) (P3HT) as a donor polymer. Environment-friendly nonhalogenated solvents were used to process large area OPVs on flexible indium tin oxide (ITO)-coated polyethylene terephthalate (PET) substrates. An alternate sequentially (Alt-Sq) blade-coated active layer with bulk heterojunction-like morphology is obtained when using $(3BS)_2$-SiPc processing with o-xylene/1,3,5-trimethylbenzene solvents. The sequential (Sq) active layer is prepared by first blade-coating $(3BS)_2$-SiPc solution followed by P3HT coated on the top without any post-treatment. The conventional sequentially (Sq) blade-coated active layer presents very low performance due to the $(3BS)_2$-SiPc bottom layer being partially washed off by processing the top layer of P3HT. In contrast, alternate sequentially (Alt-Sq) blade-coated layer-by-layer film shows even better device performance compared to the bulk heterojunction (BHJ) active layer. Time-of-flight secondary ion mass spectroscopy (TOF-SIMS) and atomic force microscopy (AFM) reveal that the Alt-Sq processing of the active layer leads to a BHJ-like morphology with a well-intermixed donor−acceptor component in the active layer while providing a simpler processing approach to low-cost and large-scale OPV production.

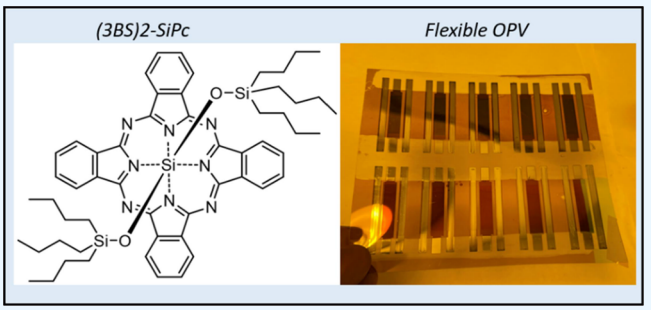

INTRODUCTION

Organic photovoltaics (OPVs) have gained significant attention due to their potential use in emerging applications such as solar sails, semitransparent curtains, and building integration.[1−4] Over the last five years, the use of non-fullerene acceptors (NFA) has enabled a significant increase in the power conversion efficiency (PCE) of OPVs reaching over 19%.[5,6] However, the majority of the champion non-fullerene acceptor materials involve multiple complex synthetic steps and result in often low yields, which will limit large-scale manufacturing and impact the cost.[7−9] The commercialization viability of OPV technology depends on the "golden triangle" rule of high PCE, long-term stability, and low cost. PCE and stability of OPVs are generally the primary focus of most research groups, while a critical factor associated with low cost, the synthetic complexity of photoactive materials, is given less consideration.[10] The synthetic complexity is defined by: (1) the number of synthetic steps, (2) reciprocal yield, (3) the number of unit operations for the isolation, (4) the number of column chromatography purification steps, and (5) the number of hazardous chemicals used in their synthesis.[11]

P3HT is one of the most popular donor polymers used in OPV applications due to its stability and ease of synthesis on a kilogram scale.[12,13] P3HT also has good solubility in many nonhalogenated solvents, providing a great opportunity for large-scale commercialization of P3HT-based OPVs.[9,14−16] NFA-based small molecules have been successfully paired with P3HT to obtain high-performance OPVs. However, the NFAs themselves have a high synthetic complexity, reducing the feasibility of the resulting combination. In order to overcome the issue of cost-effectiveness, alternative NFA must be developed for effective large-scale OPV manufacturing to take place.[8,9]

Phthalocyanines are common dye molecules which have been utilized as a semiconducting material in organic light emitting diodes,[17,18] organic thin film transistors[19−21] and organic photovoltaics.[22−27] Phthalocyanines (Pcs) are already synthesized on the ton scale annually and found in everyday textiles, paints, colorants, and inks.[28] Silicon phthalocyanine $((R)_2$-SiPc) are emerging as an exciting class of phthalocyanines due to their ability to enable n-type operation in

Received: November 4, 2022
Accepted: December 16, 2022
Published: December 29, 2022

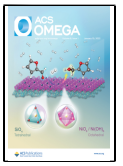

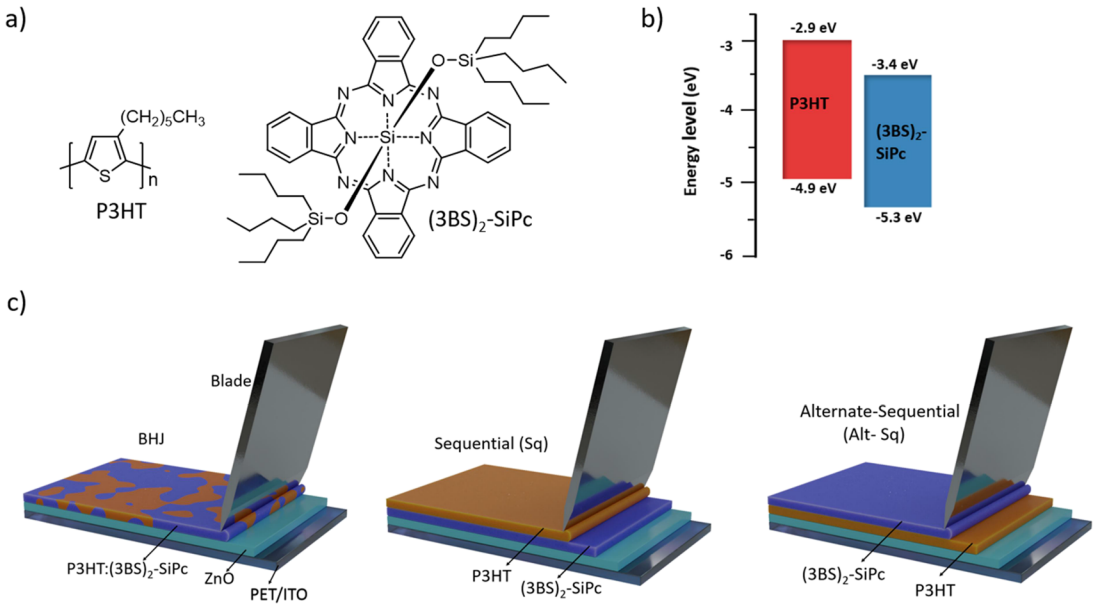

Figure 1. (a) Chemical structure of the P3HT donor and $(3BS)_2$-SiPc non-fullerene acceptor materials, (b) energy level diagram of P3HT and $(3BS)_2$-SiPc, and (c) schematic representation of inverted OPV device architecture with three types of active layer deposition of bulk heterojunction (BHJ), sequential (Sq), and alternate sequential (Alt-Sq) by blade coating.

electronics and their axial groups provide a handle to tune the physical and thermodynamic properties such as miscibility, solubility, nucleation, and solid-state arrangement.[29−33] In terms of synthetic complexity (SC), SiPcs have been reported with an SC index of 12, almost five times lower than those of high-performing NFAs such as Y6 (SC of 59) and ITIC (SC of 67).[34] Traditionally, $(R)_2$-SiPcs have been utilized as ternary additives in donor−acceptor OPVs, providing more than 20% increase in photocurrent due to the extended solar absorption[25,35−38] Recently, $(R)_2$-SiPc derivatives have also been used as NFAs with different donor polymers P3HT, PTB7, and PBDB-T and achieved high power conversion efficiencies (>4%).[39,40] These promising results demonstrate a great potential for low cost OPVs through the use of materials that have low synthetic complexity.

In this work, we aim to bring $(R)_2$-SiPcs forward as scalable NFAs. We report the large-area (1 cm^2) OPVs based on P3HT and $(3BS)_2$-SiPc NFAs acceptors using green solvents and a favorable layer-by-layer solution deposition technique by blade coating. We optimized the choice of the solvent, the processing conditions, and the deposition order. We report optimized performance as a result of alternate sequential layer-by-layer deposition. The films and resulting devices are thoroughly characterized providing morphological properties, charge transport properties, and donor−acceptor vertical stratification.

EXPERIMENTAL SECTION

Materials. P3HT was purchased from Rieke metals (4002-E, molecular weight 50−70 kDa, regioregularity 91−94%, and polydispersity index 2−2.5). $PC_{61}BM$ was purchased from Nano-C and used without any further purification. Bis(tri-n-butyl silyl oxide) silicon phthalocyanine $3(BS)_2$-SiPc) was synthesized according to previous reports.[36] Zinc oxide (ZnO) nanoparticle solution was used for the electron transport interlayer and prepared according to our previous report.[41] Molybdenum oxide (MoO_3) (>99.5%) was purchased from Sigma-Aldrich and used as received for the hole transport layer. 1,2-Dichlorobenzene (o-DCB), o-xylene, 1,3,5-trimethylbenzene (TMB), and toluene were purchased from Sigma-Aldrich.

OPV Device Fabrication. The OPV devices in this study have an inverted structure of ITO/ZnO/active layer/MoO_3/Ag. All devices were fabricated on ITO-coated, 125 μm-thick-PET sheets, purchased from Sigma Aldrich. The thickness and sheet resistance of the ITO layer are 130 nm and 60 Ω/sq, respectively. Each 15 cm × 12 cm ITO/PET sheet was patterned into 10 individual cells using a screen-printable etching paste (Solar Etch AXS Type 20). The etching paste was printed with 350-mesh stainless-steel screen using a flatbed EKRA X1-SL screen printer. The paste was cured at 120 °C for 10 min to complete the ITO etching and then washed with deionized water. The ITO-patterned sheets were afterward cleaned using sequential ultrasonication of detergent, DI water, acetone, and isopropyl alcohol for 5 min and dried on a hot plate at 120 °C. Prior to ZnO deposition, the cleaned ITO/PET sheets were treated for 30 s with oxygen plasma to change the surface energy and eliminate chemical residues. The ZnO layer was blade-coated at a blade speed of 2.5 mm/s with a blade gap of 0.3 mm, by pouring 0.25 mL volume of solution. The ZnO films (~20 nm) were then annealed at 120 °C for 10 min in ambient air.

For BHJ films, the donor−acceptor blend ink was prepared by dissolving P3HT (17 mg/mL) and R_2-SiPc with a 1:0.6 donor−acceptor weight ratio, in nonhalogenated solvents: o-xylene, TMB, and toluene. The donor and acceptor inks were prepared separately for the sequential bilayer process. P3HT (15 mg/mL) and $(3BS)_2$-SiPc) (15 mg/mL) were dissolved in o-xylene and TMB, respectively, and the solutions were stirred on a hot plate at 80 °C overnight. In Sq devices, the $(3BS)_2$-SiPc) acceptor layer was first blade-coated on top of the ZnO layer, then sequentially, P3HT was coated at different blade speeds. For alternate sequential (Alt-Sq) devices, the P3HT was first coated on top of the ZnO layer and followed sequentially by blade coating the $(3BS)_2$-SiPc) layer. All the blade-coating depositions were performed in ambient air, and the thickness of different layers was optimized by adjusting

https://doi.org/10.1021/acsomega.2c07131
ACS Omega 2023, 8, 1588−1596

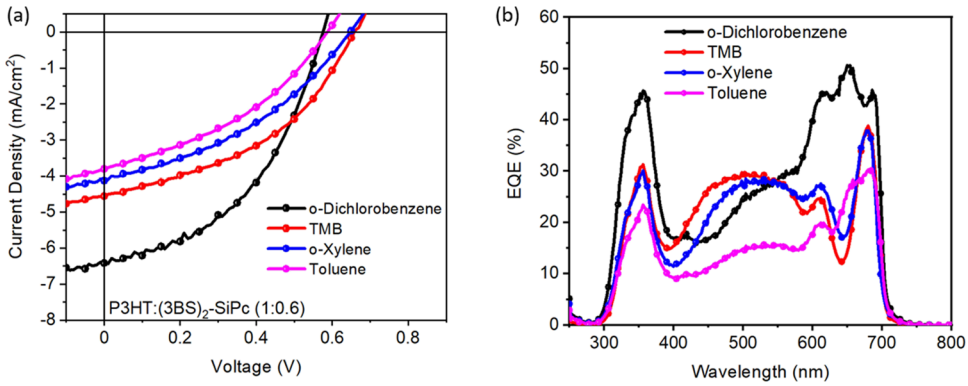

Figure 2. (a) J−V characteristics of devices with P3HT−$(3BS)_2$-SiPc (1:0.6) active layers, blade-coated from different solvents (b) corresponding EQE curves.

Table 1. OPV Device Performance Parameters of P3HT−$(3BS)_2$-SiPc (1:0.6) OPVs Prepared by Blade Coating with Different Solvents[a]

solvents	thickness (~nm)	J_{SC} (mA/cm^2)[b]	V_{OC} (V)	FF	PCE (%)
o-DCB	120 (±0.3)	−6.4 (±0.1)	0.58 (±0.03)	0.48 (±0.03)	1.8 (±0.1)
TMB	130 (±0.4)	−4.6 (±0.2)	0.66 (±0.03)	0.42 (±0.02)	1.3 (±0.1)
o-xylene	140 (±0.5)	−4.1 (±0.2)	0.63 (±0.01)	0.40 (±0.02)	1.0 (±0.1)
toluene	140 (±0.5)	−3.8 (±0.1)	0.59 (±0.02)	0.38 (±0.03)	0.8 (±0.1)

[a]All values are average with five devices, and the values in parentheses are the standard deviation. [b]Current density (J_{SC}) calculated from the EQE curve.

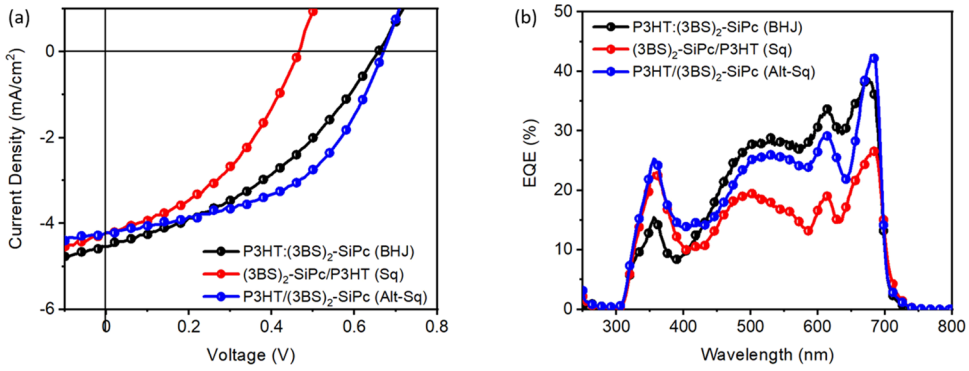

Figure 3. (a) J−V characteristics (b) corresponding EQE spectra of P3HT−$(3BS)_2$-SiPc BHJ, $3(BS)_2$-SiPc/P3HT sequential (Sq), and P3HT /$3BS)_2$-SiPc alternate sequential (Alt-Sq) devices. Active layers were blade-coated with o-xylene and TMB solvents.

blade-coating parameters, such as ink concentration, blade speed, and substrate temperature. The OPV device structure was finished by vacuum deposition (base pressure 2×10^{-7} bar) of the bilayer MoOx (10 nm) and Ag (100 nm) electrodes, having an active area of 1 cm^2. Film thicknesses were measured using a Dektak profilometer and a ZYGO NewView 7300 optical profiler.

Electrical Characterization. All characterizations of OPV devices were evaluated in ambient air at room temperature. The photovoltaic performance parameters were analyzed from the current density−voltage (J−V) characteristics. The J−V curve of OPV is measured using a Keithley 2400 digital source meter under a light intensity of 100 mW cm^{-2} corresponding to the AM 1.5G irradiation (Science Tech SS 500 W solar simulator). The solar simulator's light intensity was controlled using a calibrated Si photodiode with a KG-5 filter that was purchased from PV measurements Inc. The external quantum efficiency (EQE) spectrum was measured using a Jobin-Yvon Triax spectrometer, a xenon light source, and a Merlin lock-in amplifier. The monochromatic light intensity at each wavelength was calibrated using a standard Si UV detector and an SR570 low noise current amplifier. The short-circuit current density (J_{SC}) of all devices described in this study was verified using a wavelength integration of the EQE curve and the standard AM 1.5G solar spectrum.

Time-of-Flight Secondary Ion Spectroscopy. All three types of active layer films were analyzed using an ION-TOF (GmbH) TOF-SIMS IV that was fully equipped with a Bi cluster liquid metal ion source. In order to generate secondary ions, a 25 keV Bi_3^+ cluster primary ion beam pulsed at 10 kHz was utilized to bombard the surface of the samples. Positive or negative secondary ions were collected from the sample surface, mass-separated, and detected using a reflection-type time-of-flight analyzer, facilitating parallel monitoring of ion fragments with a mass/charge ratio (m/z) up to ~900 within 100 μs. A depth profile was obtained by repeating the cycle of alternatively sputtering the surface in an area of 100 μm × 100 μm with a 3 keV Cs^+ beam for 3 s and collecting, upon a

https://doi.org/10.1021/acsomega.2c07131
ACS Omega 2023, 8, 1588−1596

waiting time of 1 s, an ion mass spectrum using the Bi_3^+ primary ion beam at 47 × 47 pixels over an area of 128 μm × 128 μm within the sputtered area (1 shot per pixel).

RESULTS AND DISCUSSION

The chemical structures of P3HT and $(3BS)_2$-SiPc, which were used as the donor and the acceptor, respectively, in the flexible substrates using 1,2-dichlorobenzene (o-DCB) yielded comparable performances to literature values[43−45] (PCE of 2−3%) which are shown in Figure S1 and Table S1 (Supporting information). BHJ OPVs of $(3BS)_2$-SiPc and P3HT were previously optimized to PCE = 3.6% with an equal donor−acceptor weight ratio (1:1) using the spin-coating process, which served as a starting point for the optimization of this blade-coating process.[39]

Table 2. OPV Device Performance Parameters of Optimized (P3HT−$(3BS)_2$-SiPc) BHJ, ($(3BS)_2$-SiPc/P3HT) Sq, (P3HT/$(3BS)_2$-SiPc) Alt-Sq Devices under the Illumination of AM 1.5 G, 100 mW cm^{-2}[a]

active layer	J_{SC} (mA/cm^2)[b]	V_{OC} (V)	FF	PCE (%)
BHJ	−4.6 (±0.3)	0.66 (±0.01)	0.42 (±0.01)	1.3 (±0.1)
Sq	−4.1 (±0.2)	0.45 (±0.01)	0.41 (±0.02)	0.8 (±0.1)
Alt-Sq	−4.3 (±0.3)	0.67 (±0.02)	0.50 (±0.02)	1.4 (±0.1)

[a]All values are average with five devices, and the values in parentheses are the standard deviation. [b]Current density (J_{SC}) calculated from the EQE curve.

Table 3. SCLC Mobilities Obtained for P3HT−3$(BS)_2$-SiPc (BHJ, Sq, Alt-Sq Active Layers) Single Carrier Devices[a]

P3HT−(3BS)2-SiPc	μ_h [10^{-5} cm^2 V^{-1} s^{-1}]	μ_e [10^{-5} cm^2 V^{-1} s^{-1}]	μ_h/μ_e
BHJ	2.68 (± 0.6)	1.15 (± 0.2)	2.33
Sq	3.14 (± 0.7)	0.47 (± 0.2)	6.68
Alt-Sq	1.62 (± 0.2)	1.25 (± 0.2)	1.30

[a]At least four devices were taken into consideration for the averages. The active layer thickness was obtained by a dektak profilometry for mobility calculations.

fabrication of OPVs are shown in Figure 1a. The highest occupied molecular orbital/lowest unoccupied molecular orbital (HOMO/LUMO) energy levels of P3HT and $(3BS)_2$-SiPc) were taken from the literature and represented in Figure 1b.[36,42] Three different active layer configurations were optimized for device fabrication: (1) single bulk heterojunction (BHJ) layer, (2) standard sequential (Sq) bilayer deposition (acceptor then donor), and (3) alternate sequential (Alt-Sq) bilayer deposition (donor then acceptor), as shown in Figure 1c.

Baseline (P3HT−$PC_{61}BM$) devices fabricated by both spin coating on rigid ITO/glass and blade coating on ITO/PET

In this study, we optimized the performance of blade-coated P3HT−$(3BS)_2$-SiPc BHJ OPV devices by controlling the blade speed, P3HT−$(3BS)_2$-SiPc weight ratio, and substrate temperature (Figures S2,S3 and Table S2, Supporting Information). o-Xylene was used as a processing solvent. The topography and the thickness of the active layer are mainly impacted by the blade speed. When blade coating the P3HT−$(3BS)_2$-SiPc solution at a speed greater than 25 mm/s, the resulting active layer thickness was larger than 180 nm and the coated films clearly showed larger crystallites of $(3BS)_2$-SiPc (Figure S4, Supporting Information), which is not surprising, given the tendency of $(3BS)_2$-SiPc to crystalize.[36,46] However, at low blade speeds of 7.5−12.5 mm/s, the active layer films exhibit inhomogeneous thickness with larger domains of likely P3HT, which also led to poor OPV devices.

When investigating different nonchlorinated solvents, we found that the best device performance (PCE ∼ 1.3%) was achieved with P3HT−$(3BS)_2$-SiPc layers coated from the TMB solvent, with a 1:0.6 weight ratio. Figure 2 and Table 1 show J−V curves, EQE spectra, and photovoltaic parameters of P3HT−$(3BS)_2$-SiPc BHJ-based devices blade-coated with different solvents. Similar to spin-coated devices, post-thermal annealing at 110 °C for 30 min of BHJ blade-coated devices did not have a positive effect on the device performance (Figure S5, Table S3, Supporting Information).[40] This suggests that thermal annealing of the blade-coated P3HT−$(3BS)_2$-SiPc films leads to further unfavorable crystallization and phase separation.

The J−V plots and EQE spectra of optimized P3HT−$(3BS)_2$-SiPc-based BHJ, Sq, and Alt-Sq blade-coated OPVs are shown in Figure 3a,b, respectively. The extracted values of the open-circuit voltage (V_{OC}), short-circuit current density (J_{SC}), and fill factor (FF) are summarized in Table 2. The optimized BHJ OPVs coated from the TMB solvent exhibit an average V_{OC} of 0.66 V, J_{SC} of 4.6 mA/cm^2, FF of 0.42, and PCE of 1.3% (Figure S6 and Table S4, Supporting Information).

The Sq devices, processed from o-xylene, show a maximum PCE of 0.8% (Figure S7 and Table S5, Supporting

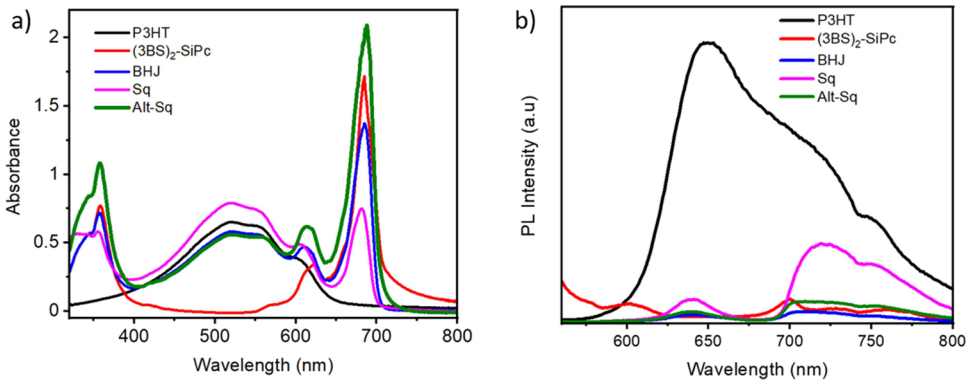

Figure 4. (a) UV−vis absorption spectra for pristine thin films of P3HT, $(3BS)_2$-SiPc, and three types of active layers (BHJ, Sq, Alt-Sq) blade-coated on PET substrates and (b) corresponding PL spectra; all films are excited at 530 nm.

https://doi.org/10.1021/acsomega.2c07131
ACS Omega 2023, 8, 1588−1596

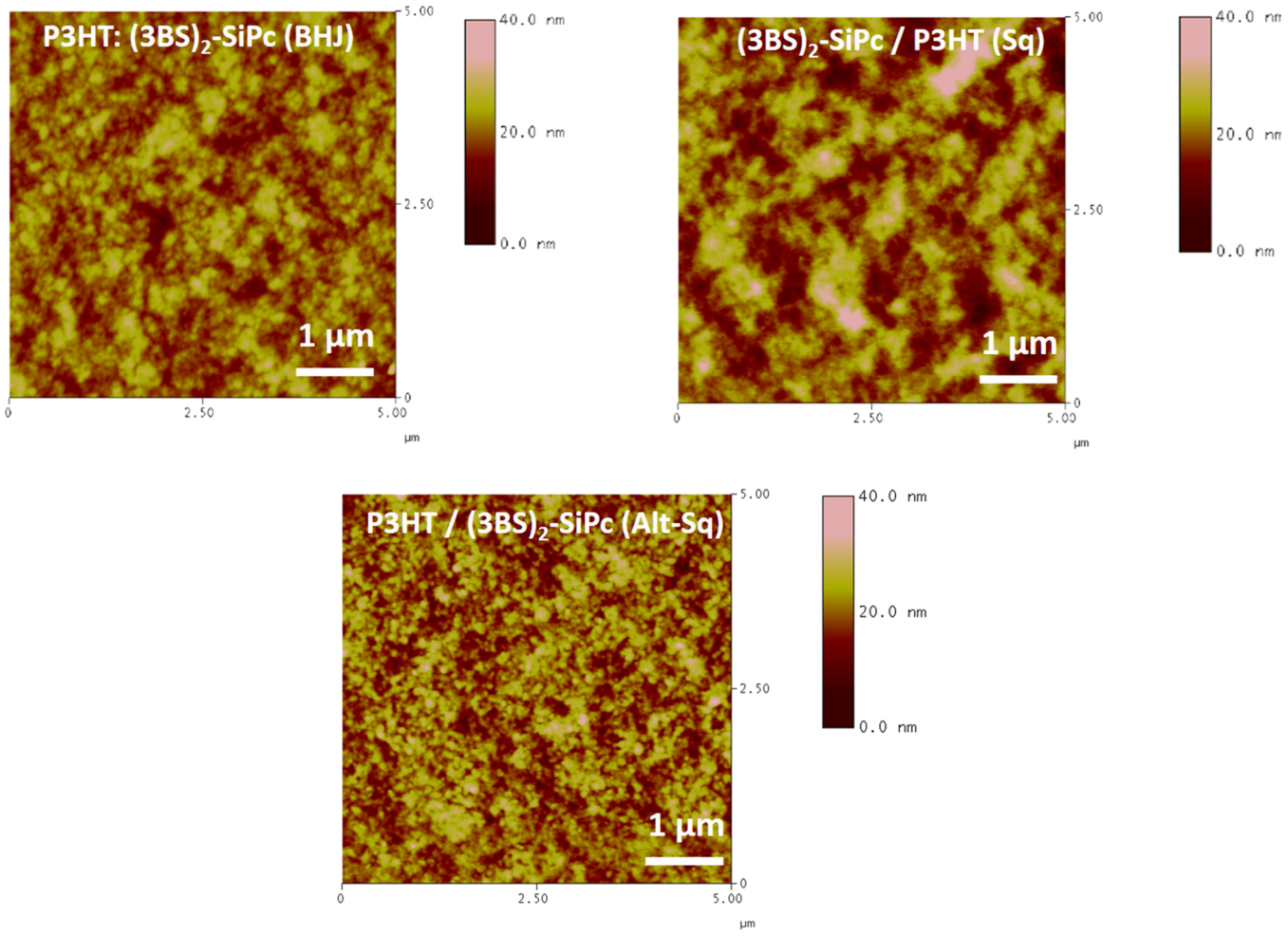

Figure 5. Tapping mode AFM height images of P3HT−$(3BS)_2$-SiPc OPVs based on three types of active layers coated on flexible substrates. Roughness of BHJ film (rms roughness = 3.1 nm); for the sequential (Sq) layer, rms roughness = 3.3 nm; for the alternate sequential (Alt-Sq) layer, rms roughness = 4.1 nm.

Information). We observed that the P3HT coating washes partially off the bottom $(3BS)_2$-SiPc layer, regardless of the solvent used. As a result, the active layer composition could not be finely tuned in order to get the optimal morphology for efficient exciton dissociation.

The Alt-Sq blade-coated devices processed with o-xylene show significantly improved photovoltaic performance with an open-circuit voltage V_{OC} of 0.67 V, J_{SC} of 4.3 mA/cm^2, FF of 0.50, and PCE of 1.4% (Figure S8 and Table S6), suggesting a favorable $(3BS)_2$-SiPc and P3HT morphology. Layer-by-layer deposition enabled further optimization of the P3HT layer through thermal annealing, prior to $(3BS)_2$-SiPc deposition, resulting in a slight improvement in PCE to 1.5%. Although Alt−Sq devices exhibit improved performance over the BHJ counterpart, the maximum FF only reached 0.50, which is comparatively low to the spin-coated BHJ devices fabricated using the o-DCB solvent. The improved performance of Alt−Sq versus BHJ using green solvents could be due to increased exciton dissociation and improved charge transport as a result of the sequentially deposited layers.[47,48]

Charge Carrier Mobility. The charge transport properties of the three types of blade-coated active layers (BHJ, Sq, Alt-Sq) were probed using the space-charge-limited current (SCLC) method. Hole (μ_h) mobilities were measured with a device structure of PET/ITO/PEDOT−PSS/active layers/MoO_3/Ag and electron (μ_e) mobilities with a device structure of PET/ITO/ZnO/active layer/Al. The charge carrier mobility was extracted by fitting the dark current versus voltage to the model of a single-carrier SCLC, which is described by the Mott-Gurney equation.[49,50]

$$J = \frac{9}{8}\mu\varepsilon_r\varepsilon_0\frac{V^2}{L^3}$$

where J is the current density, μ is the charge carrier mobility, ε_0 is the permittivity of free space, ε_r is the relative permittivity of the active layer material, L is the thickness of the films, and V is the applied voltage. The log (J−V) plot characteristics of the hole-only and electron-only devices are shown in Figure S9 and the calculated mobility values are represented as a bar chart in Figure S9 (Supporting Information) and are tabulated in Table 3.

The hole mobility (μ_h) values of optimal BHJ, Sq, and Alt-Sq devices are 2.68×10^{-5}, 3.14×10^{-5}, and 1.62×10^{-5} cm^2 V^{-1} s^{-1}, respectively, while the electron mobility (μ_e) values are 1.15×10^{-5}, 0.47×10^{-5}, and 1.25×10^{-5} cm^2 V^{-1} s^{-1}, respectively. The molecular packing and the transportation pathways have a significant impact on the charge carrier transport in OPVs.[51] The reduced μ_h and the improved μ_e in the optimal Alt-Sq devices are likely due to a better vertical phase separation of donor−acceptor in the active layer

https://doi.org/10.1021/acsomega.2c07131
ACS Omega 2023, 8, 1588−1596

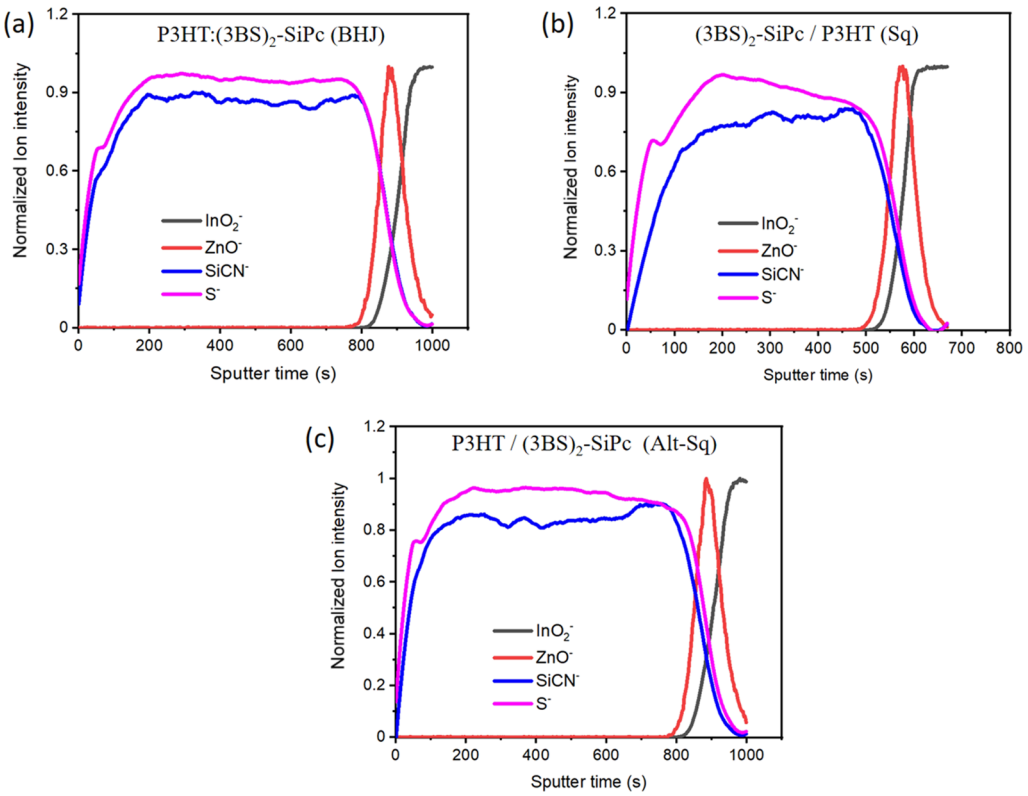

Figure 6. TOF-SIMS depth profiles of P3HT−$(3BS)_2$-SiPc OPVs (a) BHJ layer, (b) sequential (Sq), and (c) alternate sequential (Alt-Sq) photoactive layers coated on ITO substrates.

compared to BHJ and Sq devices, which will be discussed below together with other morphology parameters. As a result, a more balanced μ_h/μ_e of 1.30 was achieved for the Alt-Sq devices compared to that of 2.33 and 6.15 for the BHJ and Sq counterparts, respectively, which is consistent with the relatively larger FF (∼0.50) of the OPVs.

UV−Vis and Photoluminescence Spectra. The UV−vis absorption spectra of pristine P3HT, $(3BS)_2$-SiPc, and all OPV active layer films are shown in Figure 4a. We observe a strong characteristic absorption peak of $(3BS)_2$-SiPc at 650−700 nm (Q-band) with higher intensity in Alt-Sq film than in BHJ. This suggests that the content of $(3BS)_2$-SiPc in the Alt-Sq layer is higher, allowing good percolation pathways of $(3BS)_2$-SiPc, which is consistent with the increased electron mobility. The absorption spectrum of Sq film reveals less content of $(3BS)_2$-SiPc in the active layer, due to partial dissolution. This has an impact on the generation and dissociation of excitons and the electron mobility in the Sq configuration. Photoluminescence (PL) spectra of BHJ, Sq, Alt-Sq active layers, and neat films of P3HT and $(3BS)_2$-SiPc are shown in Figure 4b. All thin films were excited at the peak absorption of P3HT (530 nm). As expected, P3HT shows strong emission between 600 and 750 nm and no emission was detected for $(3BS)_2$-SiPc film due to the lack of absorption at 530 nm. Both BHJ and Alt-Sq films exhibit high PL quenching in the range of 600−750 nm, indicating efficient charge transfer between the P3HT and $(3BS)_2$-SiPc.

Morphology Characterization. The surface morphology of BHJ, Sq, and Alt-Sq blade-coated active layers was characterized using atomic force microscopy (AFM) (Figure 5a−c). Overall, the images reveal the active layer surfaces with root-mean-square (RMS) roughness of 3.1, 3.3, and 4.1 nm for BHJ, Sq, and Alt-Sq films, respectively. The domain size of the Alt-Sq blade-coated film is smaller than those of BHJ and Sq films, suggesting less substantial phase separation, which could be a reason for improved device performance. These fine features in the Alt-Sq blade-coated films led to a higher FF in the devices due to a better *D*/*A* interface and thus improved charge dissociation. This is also in good agreement with obtaining balanced charge carrier mobility by the SCLC method in the case of Alt-Sq blade-coated devices.

We also explored the composition of donor−acceptor in the vertical direction throughout the BHJ, Sq, and Alt-Sq films, using time-of-flight secondary ion mass spectroscopy (TOF-SIMS) (Figure 6a−c). The chemical elements through the active layers were tracked using their respective secondary ions. P3HT was tracked using sulfur ions (S^-) and silicon ions ($SiCN^-$) for the (3BS)2-SiPc acceptor, ZnO ions (ZnO^-) for the electron transport layer (ETL) layer, and indium oxide ions ($InO2^-$) for the ITO layer. There are no significant differences between BHJ and Alt-Sq active layers, suggesting that the vertical composition is very similar regardless of the process. The intensity depth profiles of S^- and $SiCN^-$ signals are identical across the whole layer, indicating that P3HT and $(3BS)_2$-SiPc are well intermixed in the active layers.

The sputter time is greater for the BHJ and Alt-Sq structures than for Sq, suggesting that the films are thicker and corroborating our initial observation that in the Sq structure, the P3HT solution dissolves the $(3BS)_2$-SiPc layer and washes it away. Sq blade-coated films also show a slight reduction in the concentration of Si^- at initial etching times (compared to Alt-Sq and BHJ), suggesting that the top of the films are less rich in $(3BS)_2$-SiPc, which is also consistent with P3HT being deposited on the top of $(3BS)_2$-SiPc. For Alt-Sq, the TOF-

https://doi.org/10.1021/acsomega.2c07131
ACS Omega 2023, 8, 1588−1596

SIMS results suggest that the $(3BS)_2$-SiPc solution does not dissolve the P3HT layer but rather swells and diffuses into the P3HT layer.[52] This result is in good agreement with balanced charge carrier transport and OPV device performance.

CONCLUSIONS

We have optimized the use of simple materials with low-synthetic complexity: P3HT and $(3BS)_2$-SiPc for the development of scalable, large-area, and flexible OPVs. The devices were fabricated using blade coating and green solvents through different deposition approaches: BHJ, Sq, and Alt-Sq. Alt-Sq deposition, where the acceptor is deposited sequentially on the top of the polymer, led to the best device performance, balanced charge carrier mobilities, and favorable morphology. Blade-coating BHJ and Alt-Sq active layers with o-xylene solution led to similar vertical distribution of the donor–acceptor morphology, suggesting that similar performance can be obtained by both techniques. Typically, Alt-Sq deposition is favored industrially over BHJ as each layer can be independently optimized rather than trying to optimize a more complex blend. These results demonstrate significant steps toward large-scale implementation of silicon phthalocyanines in low-cost, flexible OPVs.

ASSOCIATED CONTENT

Supporting Information

The Supporting Information is available free of charge at https://pubs.acs.org/doi/10.1021/acsomega.2c07131.

Descriptions of three types of active layer device structures; full device optimization; and resulting device performance parameters (PDF)

AUTHOR INFORMATION

Corresponding Authors

Salima Alem − *Advanced Electronics and Photonics Research Centre, National Research Council of Canada, Ottawa, ON K1A 0R6, Canada*; Email: salima.alem@nrc-cnrc.gc.ca

Benoît H. Lessard − *Department of Chemical & Biological Engineering, University of Ottawa, Ottawa, ON K1N 6N5, Canada; School of Electrical Engineering and Computer Science, University of Ottawa, Ottawa, ON K1N 6N5, Canada*; orcid.org/0000-0002-9863-7039; Email: benoit.lessard@uottawa.ca

Authors

Chithiravel Sundaresan − *Department of Chemical & Biological Engineering, University of Ottawa, Ottawa, ON K1N 6N5, Canada; Advanced Electronics and Photonics Research Centre, National Research Council of Canada, Ottawa, ON K1A 0R6, Canada*

Mário C. Vebber − *Department of Chemical & Biological Engineering, University of Ottawa, Ottawa, ON K1N 6N5, Canada*

Jaclyn L. Brusso − *Department of Chemistry and Biomolecular Science, University of Ottawa, Ottawa, ON K1N 6N5, Canada*; orcid.org/0000-0001-9959-2015

Ye Tao − *Advanced Electronics and Photonics Research Centre, National Research Council of Canada, Ottawa, ON K1A 0R6, Canada*

Complete contact information is available at: https://pubs.acs.org/10.1021/acsomega.2c07131

Notes

The authors declare no competing financial interest.

ACKNOWLEDGMENTS

The authors thank Dr. Jianping Lu, Dr. Stephen Lang, Mr. Eric Estwick, and Mrs. Simona Moisa from National Research Council Canada for their technical support. The authors also thank Dr. Hang-Yong Nie at Surface Science Western (University of Western Ontario) for TOF-SIMS study. The Natural sciences and engineering research council of Canada (NSERC, RGPIN/2015-50 903 987 to B.H.L.) and the university of Ottawa are acknowledged for their financial support. This work was supported by the NSERC Green Electronics Network (GreEN) (grant no.: NETGP 508 526-17 to B.H.L.).

REFERENCES

(1) Lipomi, D. J.; Bao, Z. Stretchable, Elastic Materials and Devices for Solar Energy Conversion. *Energy Environ. Sci.* **2011**, *4*, 3314–3328.

(2) Li, Y.; Guo, X.; Peng, Z.; Qu, B.; Yan, H.; Ade, H.; Zhang, M.; Forrest, S. R. Color-Neutral, Semitransparent Organic Photovoltaics for Power Window Applications. *Proc. Natl. Acad. Sci. U. S. A.* **2020**, *117*, 21147–21154.

(3) Lee, B.; Lahann, L.; Li, Y.; Forrest, S. R. Cost Estimates of Production Scale Semitransparent Organic Photovoltaic Modules for Building Integrated Photovoltaics. *Sustain. Energy Fuels* **2020**, *4*, 5765–5772.

(4) Hu, Z.; Wang, J.; Ma, X.; Gao, J.; Xu, C.; Yang, K.; Wang, Z.; Zhang, J.; Zhang, F. A Critical Review on Semitransparent Organic Solar Cells. *Nano Energy* **2020**, *78*, No. 105376.

(5) Zhu, L.; Zhang, M.; Xu, J.; Li, C.; Yan, J.; Zhou, G.; Zhong, W.; Hao, T.; Song, J.; Xue, X.; Zhou, Z.; Zeng, R.; Zhu, H.; Chen, C. C.; MacKenzie, R. C. I.; Zou, Y.; Nelson, J.; Zhang, Y.; Sun, Y.; Liu, F. Single-Junction Organic Solar Cells with over 19% Efficiency Enabled by a Refined Double-Fibril Network Morphology. *Nat. Mater.* **2022**, *21*, 656–663.

(6) Cui, Y.; Yao, H.; Zhang, J.; Xian, K.; Zhang, T.; Hong, L.; Wang, Y.; Xu, Y.; Ma, K.; An, C.; He, C.; Wei, Z.; Gao, F.; Hou, J. Single-Junction Organic Photovoltaic Cells with Approaching 18% Efficiency. *Adv. Mater.* **2020**, *32*, No. e1908205.

(7) Wadsworth, A.; Moser, M.; Marks, A.; Little, M. S.; Gasparini, N.; Brabec, C. J.; Baran, D.; McCulloch, I. Critical Review of the Molecular Design Progress in Non-Fullerene Electron Acceptors towards Commercially Viable Organic Solar Cells. *Chem. Soc. Rev.* **2019**, *48*, 1596–1625.

(8) Yang, C.; Zhang, S.; Ren, J.; Gao, M.; Bi, P.; Ye, L.; Hou, J.; Zhang, S.; Ye, L.; Hou, J. Molecular Design of a Non-Fullerene Acceptor Enables a P3HT-Based Organic Solar Cell with 9.46% Efficiency. *Energy Environ. Sci.* **2020**, *13*, 2864–2869.

(9) Xu, X.; Zhang, G.; Yu, L.; Li, R.; Peng, Q. P3HT-Based Polymer Solar Cells with 8.25% Efficiency Enabled by a Matched Molecular Acceptor and Smart Green-Solvent Processing Technology. *Adv. Mater.* **2019**, *31*, No. e1906045.

(10) Po, R.; Bianchi, G.; Carbonera, C.; Pellegrino, A. "all That Glisters Is Not Gold:" An Analysis of the Synthetic Complexity of Efficient Polymer Donors for Polymer Solar Cells. *Macromolecules* **2015**, *48*, 453–461.

(11) Moser, M.; Wadsworth, A.; Gasparini, N.; McCulloch, I. Challenges to the Success of Commercial Organic Photovoltaic Products. *Adv. Energy Mater.* **2021**, *11*, No. 2100056.

(12) Holliday, S.; Ashraf, R. S.; Wadsworth, A.; Baran, D.; Yousaf, S. A.; Nielsen, C. B.; Tan, C. H.; Dimitrov, S. D.; Shang, Z.; Gasparini, N.; Alamoudi, M.; Laquai, F.; Brabec, C. J.; Salleo, A.; Durrant, J. R.; McCulloch, I. High-Efficiency and Air-Stable P3HT-Based Polymer Solar Cells with a New Non-Fullerene Acceptor. *Nat. Commun.* **2016**, *7*, 11585.

(13) Po, R.; Bernardi, A.; Calabrese, A.; Carbonera, C.; Corso, G.; Pellegrino, A. From Lab to Fab: How Must the Polymer Solar Cell Materials Design Change?-An Industrial Perspective. *Energy Environ. Sci.* **2014**, *7*, 925−943.
(14) Xiao, B.; Tang, A.; Zhang, Q.; Li, G.; Wang, X.; Zhou, E. A2-A1-D-A1-A2 Type Non-Fullerene Acceptors with 2-(1,1-Dicyanomethylene)Rhodanine as the Terminal Groups for Poly(3-Hexylthiophene)-Based Organic Solar Cells. *ACS Appl. Mater. Interfaces* **2018**, *10*, 34427−34434.
(15) Baran, D.; Ashraf, R. S.; Hanifi, D. A.; Abdelsamie, M.; Gasparini, N.; Röhr, J. A.; Holliday, S.; Wadsworth, A.; Lockett, S.; Neophytou, M.; Emmott, C. J. M.; Nelson, J.; Brabec, C. J.; Amassian, A.; Salleo, A.; Kirchartz, T.; Durrant, J. R.; McCulloch, I. Reducing the Efficiency-Stability-Cost Gap of Organic Photovoltaics with Highly Efficient and Stable Small Molecule Acceptor Ternary Solar Cells. *Nat. Mater.* **2017**, *16*, 363−369.
(16) Guo, X.; Zhang, M.; Cui, C.; Hou, J.; Li, Y. Efficient Polymer Solar Cells Based on Poly(3-Hexylthiophene) and Indene-C60 Bisadduct Fabricated with Non-Halogenated Solvents. *ACS Appl. Mater. Interfaces* **2014**, *6*, 8190−8198.
(17) Plint, T.; Lessard, B. H.; Bender, T. P. Assessing the Potential of Group 13 and 14 Metal/Metalloid Phthalocyanines as Hole Transport Layers in Organic Light Emitting Diodes. *J. Appl. Phys.* **2016**, *119*, 145502.
(18) Pearson, A. J.; Plint, T.; Jones, S. T. E.; Lessard, B. H.; Credgington, D.; Bender, T. P.; Greenham, N. C. Silicon Phthalocyanines as Dopant Red Emitters for Efficient Solution Processed OLEDs. *J. Mater. Chem. C* **2017**, *5*, 12688−12698.
(19) Melville, O. A.; Grant, T. M.; Lessard, B. H. Silicon Phthalocyanines as N-Type Semiconductors in Organic Thin Film Transistors. *J. Mater. Chem. C* **2018**, *6*, 5482−5488.
(20) Melville, O. A.; Grant, T. M.; Mirka, B.; Boileau, N. T.; Park, J.; Lessard, B. H. Ambipolarity and Air Stability of Silicon Phthalocyanine Organic Thin-Film Transistors. *Adv. Electron. Mater.* **2019**, *5*, No. 1900087.
(21) King, B.; Melville, O. A.; Rice, N. A.; Kashani, S.; Tonnelé, C.; Raboui, H.; Swaraj, S.; Grant, T. M.; McAfee, T.; Bender, T. P.; Ade, H.; Castet, F.; Muccioli, L.; Lessard, B. H. Silicon Phthalocyanines for N-Type Organic Thin-Film Transistors: Development of Structure−property Relationships. *ACS Appl. Electron. Mater.* **2021**, *3*, 325−336.
(22) Zysman-Colman, E.; Ghosh, S. S.; Xie, G.; Varghese, S.; Chowdhury, M.; Sharma, N.; Cordes, D. B.; Slawin, A. M. Z.; Samuel, I. D. W. Solution-Processable Silicon Phthalocyanines in Electroluminescent and Photovoltaic Devices. *ACS Appl. Mater. Interfaces* **2016**, *8*, 9247−9253.
(23) Ke, L.; Gasparini, N.; Min, J.; Zhang, H.; Adam, M.; Rechberger, S.; Forberich, K.; Zhang, C.; Spiecker, E.; Tykwinski, R. R.; Brabec, C. J.; Ameri, T. Panchromatic Ternary/Quaternary Polymer/Fullerene BHJ Solar Cells Based on Novel Silicon Naphthalocyanine and Silicon Phthalocyanine Dye Sensitizers. *J. Mater. Chem. A* **2017**, *5*, 2550−2562.
(24) Lessard, B. H.; White, R. T.; Al-Amar, M.; Plint, T.; Castrucci, J. S.; Josey, D. S.; Lu, Z. H.; Bender, T. P. Assessing the Potential Roles of Silicon and Germanium Phthalocyanines in Planar Heterojunction Organic Photovoltaic Devices and How Pentafluoro Phenoxylation Can Enhance π-π Interactions and Device Performance. *ACS Appl. Mater. Interfaces* **2015**, *7*, 5076−5088.
(25) Sundaresan, C.; Alem, S.; Radford, C. L.; Grant, T. M.; Kelly, T. L.; Lu, J.; Tao, Y.; Lessard, B. H. Changes in Optimal Ternary Additive Loading When Processing Large Area Organic Photovoltaics by Spin- versus Blade-Coating Methods. *Sol. RRL* **2021**, *5*, No. 2100432.
(26) Faure, M.; Grant, T.; Lessard, B. Silicon Phthalocyanines as Acceptor Candidates in Mixed Solution/Evaporation Processed Planar Heterojunction Organic Photovoltaic Devices. *Coatings* **2019**, *9*, 203.
(27) Ke, L.; Min, J.; Adam, M.; Gasparini, N.; Hou, Y.; Perea, J. D.; Chen, W.; Zhang, H.; Fladischer, S.; Sale, A. C.; Spiecker, E.; Tykwinski, R. R.; Brabec, C. J.; Ameri, T. A Series of Pyrene-Substituted Silicon Phthalocyanines as Near-IR Sensitizers in Organic Ternary Solar Cells. *Adv. Energy Mater.* **2016**, *6*, No. 1502355.
(28) Lomax, S. Q. Phthalocyanine and Quinacridone Pigments: Their History, Properties and Use. *Stud. Conserv.* **2005**, *50*, 19−29.
(29) Vebber, M. C.; Rice, N. A.; Brusso, J. L.; Lessard, B. H. Thermodynamic Property-Performance Relationships in Silicon Phthalocyanine-Based Organic Photovoltaics. *ACS Appl. Energy Mater.* **2022**, *5*, 3426−3435.
(30) Dindault, C.; King, B.; Williams, P.; Absi, J. H.; Faure, M. D. M.; Swaraj, S.; Lessard, B. H. Correlating Morphology, Molecular Orientation, and Transistor Performance of Bis-(Pentafluorophenoxy)Silicon Phthalocyanine Using Scanning Transmission X-Ray Microscopy. *Chem. Mater.* **2022**, *34*, 4496.
(31) Lessard, B. H. The Rise of Silicon Phthalocyanine: From Organic Photovoltaics to Organic Thin Film Transistors. *ACS Appl. Mater. Interfaces* **2021**, *13*, 31321−31330.
(32) Cranston, R. R.; Vebber, M. C.; Rice, N. A.; Tonnelé, C.; Castet, F.; Muccioli, L.; Brusso, J. L.; Lessard, B. H. N-Type Solution-Processed Tin versus Silicon Phthalocyanines: A Comparison of Performance in Organic Thin-Film Transistors and in Organic Photovoltaics. *ACS Appl. Electron. Mater.* **2021**, *3*, 1873−1885.
(33) Cranston, R. R.; King, B.; Dindault, C.; Grant, T. M.; Rice, N. A.; Tonnelé, C.; Muccioli, L.; Castet, F.; Swaraj, S.; Lessard, B. H. Highlighting the Processing Versatility of a Silicon Phthalocyanine Derivative for Organic Thin-Film Transistors. *J. Mater. Chem. C* **2022**, *10*, 485−495.
(34) Vebber, M. C.; Rice, N. A.; Brusso, J. L.; Lessard, B. H. Variance-Resistant PTB7 and Axially-Substituted Silicon Phthalocyanines as Active Materials for High-Voc Organic Photovoltaics. *Sci. Rep.* **2021**, *11*, 15347.
(35) Honda, S.; Ohkita, H.; Benten, H.; Ito, S. Selective Dye Loading at the Heterojunction in Polymer/Fullerene Solar Cells. *Adv. Energy Mater.* **2011**, *1*, 588−598.
(36) Dang, M. T.; Grant, T. M.; Yan, H.; Seferos, D. S.; Lessard, B. H.; Bender, T. P. Bis(Tri-n-Alkylsilyl Oxide) Silicon Phthalocyanines: A Start to Establishing a Structure Property Relationship as Both Ternary Additives and Non-Fullerene Electron Acceptors in Bulk Heterojunction Organic Photovoltaic Devices. *J. Mater. Chem. A* **2017**, *5*, 12168−12182.
(37) Vebber, M. C.; Grant, T. M.; Brusso, J. L.; Lessard, B. H. Bis(Trialkylsilyl Oxide) Silicon Phthalocyanines: Understanding the Role of Solubility in Device Performance as Ternary Additives in Organic Photovoltaics. *Langmuir* **2020**, *36*, 2612−2621.
(38) Sundaresan, C.; Josse, P.; Vebber, M. C.; Brusso, J.; Lu, J.; Tao, Y.; Alem, S.; Lessard, B. H. Design of Ternary Additive for Organic Photovoltaics: A Cautionary Tale. *RSC Adv.* **2022**, *12*, 10029−10036.
(39) Grant, T. M.; Kaller, K. L. C.; Coathup, T. J.; Rice, N. A.; Hinzer, K.; Lessard, B. H. High Voc Solution-Processed Organic Solar Cells Containing Silicon Phthalocyanine as a Non-Fullerene Electron Acceptor. *Org. Electron.* **2020**, *87*, 105976.
(40) Grant, T. M.; Dindault, C.; Rice, N. A.; Swaraj, S.; Lessard, B. H. Synthetically Facile Organic Solar Cells with >4% Efficiency Using P3HT and a Silicon Phthalocyanine Non-Fullerene Acceptor. *Mater. Adv.* **2021**, *2*, 2594−2599.
(41) Alem, S.; Lu, J.; Movileanu, R.; Kololuoma, T.; Dadvand, A.; Tao, Y. Solution-Processed Annealing-Free ZnO Nanoparticles for Stable Inverted Organic Solar Cells. *Org. Electron.* **2014**, *15*, 1035−1042.
(42) Chen, D.; Yang, Y.; Zhong, C.; Yi, Z.; Wu, F.; Qu, L.; Li, Y.; Li, Y.; Qin, J. Synthesis and Photovoltaic Properties of Two-Dimensional D-A Copolymers with Conjugated Side Chains. *J. Polym. Sci. Part A Polym. Chem.* **2011**, *49*, 3852−3862.
(43) Zhou, Y.; Zhang, F.; Tvingstedt, K.; Barrau, S.; Li, F.; Tian, W.; Inganäs, O. Investigation on Polymer Anode Design for Flexible Polymer Solar Cells. *Appl. Phys. Lett.* **2008**, *92*, 233308.
(44) Schmidt-Hansberg, B.; Sanyal, M.; Klein, M. F. G.; Pfaff, M.; Schnabel, N.; Jaiser, S.; Vorobiev, A.; Müller, E.; Colsmann, A.; Scharfer, P.; Gerthsen, D.; Lemmer, U.; Barrena, E.; Schabel, W. Moving through the Phase Diagram: Morphology Formation in

https://doi.org/10.1021/acsomega.2c07131
ACS Omega 2023, 8, 1588−1596

Solution Cast Polymer-Fullerene Blend Films for Organic Solar Cells. *ACS Nano* **2011**, *5*, 8579−8590.
(45) Kang, H.; Kim, G.; Kim, J.; Kwon, S.; Kim, H.; Lee, K. Bulk-Heterojunction Organic Solar Cells: Five Core Technologies for Their Commercialization. *Adv. Mater.* **2016**, *28*, 7821−7861.
(46) Lessard, B. H.; Dang, J. D.; Grant, T. M.; Gao, D.; Seferos, D. S.; Bender, T. P. Bis(Tri- n -Hexylsilyl Oxide) Silicon Phthalocyanine: A Unique Additive in Ternary Bulk Heterojunction Organic Photovoltaic Devices. *ACS Appl. Mater. Interfaces* **2014**, *6*, 15040−15051.
(47) Guo, S.; Hu, Y.; Qin, M.; Li, J.; Wang, Y.; Qin, J.; Cheng, P. Toward High-Performance Organic Photovoltaics: The New Cooperation of Sequential Solution-Processing and Promising Non-Fullerene Acceptors. *Mater. Horiz.* **2022**, *9*, 2097−2108.
(48) Liu, Z.; Ma, X.; Xu, W.; Zhang, S.; Xu, C.; Young Jeong, S.; Young Woo, H.; Zhou, Z.; Zhang, F. 15.28% Efficiency of Conventional Layer-By-Layer All-Polymer Solar Cells Superior To Bulk Heterojunction or Inverted Cells. *Chem. Eng. J.* **2022**, *450*, 138146.
(49) Bozano, L.; Carter, S. A.; Scott, J. C.; Malliaras, G. G.; Brock, P. J. Temperature- and Field-Dependent Electron and Hole Mobilities in Polymer Light-Emitting Diodes. *Appl. Phys. Lett.* **1999**, *74*, 1132−1134.
(50) Li, X.; Pan, F.; Sun, C.; Zhang, M.; Wang, Z.; Du, J.; Wang, J.; Xiao, M.; Xue, L.; Zhang, Z. G.; Zhang, C.; Liu, F.; Li, Y. Simplified Synthetic Routes for Low Cost and High Photovoltaic Performance N-Type Organic Semiconductor Acceptors. *Nat. Commun.* **2019**, *10*, 519.
(51) Cheng, P.; Wang, R.; Zhu, J.; Huang, W.; Chang, S. Y.; Meng, L.; Sun, P.; Cheng, H. W.; Qin, M.; Zhu, C.; Zhan, X.; Yang, Y. Ternary System with Controlled Structure: A New Strategy toward Efficient Organic Photovoltaics. *Adv. Mater.* **2018**, *30*, No. 1705243.
(52) Ren, M.; Zhang, G.; Chen, Z.; Xiao, J.; Jiao, X.; Zou, Y.; Yip, H. L.; Cao, Y. High-Performance Ternary Organic Solar Cells with Controllable Morphology via Sequential Layer-by-Layer Deposition. *ACS Appl. Mater. Interfaces* **2020**, *12*, 13077−13086.

https://doi.org/10.1021/acsomega.2c07131
ACS Omega 2023, 8, 1588−1596